© 2017. This manuscript version is made available under the CC-BY-NC-ND 4.0 license http://creativecommons.org/licenses/by-nc-nd/4.0/
Published Journal Article available at: https://doi.org/10.1016/j.jweia.2017.09.016

Wind tunnel experiment on a heavy truck equipped with front-rear trailer device

L. Salati *, P. Schito, F. Cheli

Dipartimento di Meccanica, Politecnico di Milano, Via la Masa 1, Milano, Italy

The aerodynamic drag of a "common" European heavy truck equipped with Front-Rear trailer device, earlier designed by the authors with numerical simulations, was investigated through wind tunnel testing on a 1:10 scale model.

The device, placed on the top and sides of the trailer, as well as at the front and rear, increases the overall dimensions of the heavy truck by less than 1% in width and height, and reduces the overall drag by about 10%. The Front-Rear trailer device was separated into several parts (top, side, front and rear) to analyze which one reduced the drag more. An analysis was carried out on several parts of the same device simultaneously installed on the trailer (for example top-front and top-rear devices mounted at the same time), in addition to an analysis of the performance of the Front trailer device based on the length of the device itself. Tests were performed both in front wind and crosswind conditions.

The device is expected to generate a consistent drag reduction both in front wind and crosswind, to reduce greenhouse gas and pollutant emissions.

1. Introduction

It is estimated that 50% of the truck engine power is needed to overcome the aerodynamic drag of a Heavy Goods Vehicle (HGV) at a typical highway speed of *90-100 km/h* Schoon (2007). In fact, aerodynamic drag increases in relation to the square of the vehicle speed, and drag is the main source of fuel consumption at cruise speed. Aerodynamic efficiency is strongly affected by the regulation concerning the maximum vehicle dimensions. In Europe, the legal maximum vehicle length includes the whole heavy truck (Directive 96/53/EC (The Council of The European Union, 1996)), influencing especially the tractor shape and its aerodynamics performance. In other countries, as in the US, only the trailer length is fixed, allowing the shape of the tractor to be more streamlined as shown in Fig. 1.

A first way to reduce drag in heavy trucks without any modification to the HGV geometry is platooning as shown in Schito and Braghin (2012). Platooning is the strategy of coupling two or more vehicles together while they are travelling on the highway at a distance between 5 m and 15 m. Several studies were done to understand the impact of this driving strategy on the environment, traffic safety and traffic congestion. Among which, the Safe Road Trains for the Environment (SARTRE) (Dávila and Nombela, 2011) is a European project aimed at studying platooning to include also passenger vehicles. The main goal is to determine if platooning can be integrated with non-platoon traffic, lane changes, etc. Platooning gives promising results, but it requires a significant change in the infrastructure and in the driving behavior of the vehicles traveling in the platoon configuration. For all these reasons, commercial platooning is currently not available.

There are several strategies for reducing the drag on a heavy truck. They can be separated into two major categories: those installed on the tractor and those installed on the trailer. As described in Leuschen and Cooper (2006), there could exist as many devices as the number of tractors and trailers in service. Most drag reduction devices are designed to be mounted on the trailer. There is normally a reluctance in industry to adopt them, as a marked distinction exists between tractor owners/operators and those of trailers. Nevertheless, trailer manufacturers (in addition to operators in general) have little interest in these devices that increase the overall acquisition costs of the trailer.

As a result of studies on the aerodynamic efficiency of a single HGV vehicle, it is known that aerodynamic drag is mostly influenced by:

- the front corner radius of the tractor (Palowski, 1930);
- the tractor-trailer gap (Hucho, 1987);
- the underbody of both trailer and tractor (Buchheim et al., 1981; Howell, 1994;
- the aerodynamic interaction between the tractor and the trailer (Gilhaus, 1980).

Given this information, several aerodynamic devices are currently used to reduce the drag of the trailer, the most common ones being:

Received 8 November 2016;
Received in revised form 22 September 2017;
Accepted 22 September 2017

* Corresponding author.
E-*mail addresses:* luigi.salati@polimi.it (L. Salati), paolo.schito@polimi.it (P. Schito), federico.cheli@polimi.it (F. Cheli).

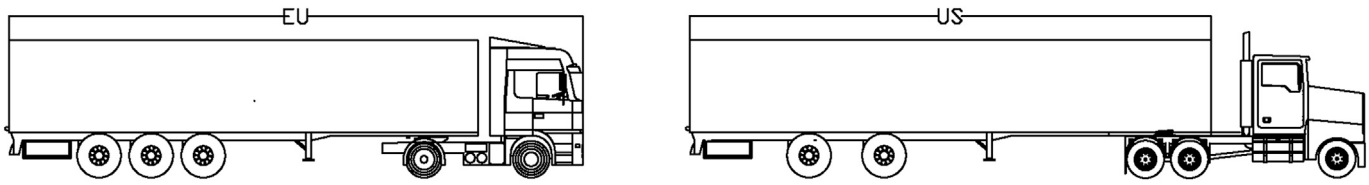

Fig. 1. Comparison between European and America regulations regarding heavy truck maximum dimension.

- cab roof fairings and side fairings (9–17% drag reduction - Drollinger, 1987; Cooper, 2003; Leuschen and Cooper, 2009);
- trailer–front fairing (7–10% drag reduction - Garry, 1981; Watkins et al., 1993);
- tractor and trailer side-skirts (4–6% drag reduction – Garry, 1985; Ingram, 1978).

Normally, heavy trucks have a simple two box shape, where one box (tractor + trailer) is located in front of the other.

The first way to reduce drag is to design the front corner radius of the first box in a proper way so as to maintain the flow attached to the sides of the tractor.

The tractor-trailer gap is defined as the area between the rear of the tractor and the front of the trailer. This area needs to be analyzed to avoid the stepped shape existing in the side elevation of the vehicle, and to avoid the pressure drop in the front part of the trailer, both of which strongly produce drag.

Rounding the front edges of the driving cab will generally reduce drag. Sometimes the flow separates at the top of the tractor, then it impinges on the front of the trailer and separates again along the front trailer edge. For this reason, sometimes, a shaper angle on the driving cab can generate an earlier separation that moves the flow directly over the front face of the trailer, generating a strong drag reduction. With European trucks, in particular, this problem is avoided by designing cab roof fairings.

Nevertheless, the tractor-trailer gap on the sides of the vehicle needs to be correctly designed, especially when the vehicle is running in a crosswind condition. If the yaw angle (the angle between the vehicle speed and the wind direction) becomes relevant, free-stream wind can pass between the driving cab and the trailer. In this condition, the drag of the vehicle is the sum of the drag of two separate bluff bodies, while in the front wind condition, it is normally lower (one box shields the other). To avoid this problem and control the flow-field between the two bluff bodies, side fairings are installed on the driving cab. For this reason, the clearance gap that should be provided between the tractor and the trailer strongly influences the aerodynamic performance of the vehicle. If the gap is very small, the aerodynamic efficiency will be very high but the turning capacity of the vehicle will be strongly affected, since the trailer may collide with the driving cab, while with a large gap, the vehicle tends to behave as two separate bodies that generate twice the drag of a single body. This effect is amplified in crosswind conditions, when the vehicle is yawed with respect to the wind direction (Gilhaus, 1980).

Landman et al. (2010) has suggested that addressing the gap issue completely would produce a drag saving of approximately 6% for a typical tractor-trailer and would save approximately 3% of fuel at 98 km/h.

When the driving cab is properly designed and the tractor-trailer gap is properly managed, the main sources of drag are in the underbody section and at the rear of the trailer.

The open area below the trailer generates high drag, especially in crosswind. The most common approach is to prevent the air from entering by installing side skirts along the HGV.

The vortices located at the rear of the trailer have different lengths: the dimension of the top-rear vortex is almost that of the bottom-rear one, with the flow-field at the top of the vehicle being almost the same as the free-stream speed, while in the bottom the flow is influenced by the underbody of the HGV, suggesting that it could be convenient to realize a device for this non symmetric flow on the zero X-Z plane (according to the reference system in Fig. 6-b).

In the past, several other devices that exceed the maximum allowed dimensions of the vehicle were designed to modify the flow-field in the rear part of the trailer. It is not possible to use a truck having larger dimensions than those prescribed, therefore a tradeoff must be performed between the loading capacity of the trailer and its aerodynamic efficiency. It should be said that the loading capacity modification is generally not considered, therefore a different way to exceed the allowed dimensions must be found. From among other devices, boat-tails are located at the rear of the vehicle, exceeding the maximum vehicle length. They reduce the overall aerodynamic loss and achieve a drag reduction of around 7.5% (McCallen et al., 2004; Cooper, 2003).

In the author's previous works (Salati et al., 2015) the Front-Rear trailer devices were developed using CFD (Computational Fluid Dynamics) analysis. This passive device, with an elliptic shape, is located in the front and rear sections of the trailer (both on the top and on the sides). Even though it reduces the overall vehicle drag by about 12%, but it also increases the maximum height and width of the vehicle by 5.0 cm.

A study by the Institute of Aerospace Research at the National Research Council (NRC-IAR) (Leuschen and Cooper, 2009) demonstrated that, for an average heavy vehicle operated in Canada and US, removing the side mirrors from the HGV would save 938 L of fuel annually per truck.

The main risk with side view cameras instead of traditional mirrors is reliability. Without considering accidental damage, side mirrors have a service life that exceeds the service life of the heavy truck. On the contrary, side view cameras introduce several electrical components, each one having and independent own service life which is lower than that of the mirrors. In addition, there must be the need for cameras to have some system redundancy in case of failure. This redundancy should be positioned in a way that does not affect the aerodynamics of the vehicle when not being used.

In recent years, many studies have been performed on active drag reduction devices, such as boundary layer suction (as an example Minelli et al., 2016), but their complexity and the necessity to provide energy for their operation (to be compared with the energy benefit in order to make a profitable energy balance) has not yet permitted these devices to reach the market.

Quite often, an HGV travels with containers for shipping. This kind of trailer is diffused in the worldwide economy, but is also inefficient from an aerodynamic point of view: its sharp step side shape, needed for structural reasons, is a high source of drag for the vehicle.

The aerodynamics of heavy trucks is not only important for fuel saving, but also for preventing wind induced accidents when the vehicle is driving in crosswind. Heavy trucks, due to their large lateral area, are very sensitive to crosswind and overturning. It is not desirable that an increase in efficiency leads to an increased sensitivity to lateral winds effect.

External devices, installed on the trailer, also need to be studied in crosswind to carefully control their effect on the overall vehicle aerodynamics and on its stability, especially in crosswind.

In this paper, the performance of the Front-Rear trailer devices developed by the authors (Salati et al., 2015) was tested in wind tunnel experiments on a truck of scale 1:10 scale truck both in front

and crosswind.

2. Experimental set-up

2.1. Target vehicle

It was decided to use a target vehicle corresponding to a common truck currently available on the EU roads. The vehicle is a simplified model of a real one, with the main aerodynamically significant details considered: the cooling system and connections between wheel axels and chassis were simplified, as well as the indicators and the vehicle registration holder plate (see Fig. 2).

The base model was already provided with commonly installed aerodynamic devices, such as cab roof fairings, side fairings, wheel houses for the tractor tires and a suitable design of the front corner radius of the tractor. The model was built on a scale of 1:10 compared to the real one, making it possible to manufacture all HGV details that may influence the aerodynamic forces. The dimensions and the sign conventions are reported in Fig. 2.

The HGV was divided into several separate parts: a part of the trailer was made of a wooden frame of Oriented Strand Board (OSB) (drawn in blue in Fig. 3), while the truck was made of polymer material modelled using a 5-axis CNC machine (drawn in black in Fig. 3). The part of the trailer shielded by the devices and the devices themselves were made from one polymeric component that was modelled using a 5-axis CNC machine (drawn in pink in Fig. 3). In this way, it was possible to have an accurate device shape and keep the edge between the device and trailer sharp. The cab roof fairings, the side fairings and the wheels were made of plastic (drawn in red in Fig. 3).

With this kind of construction, a more realistic tractor-trailer gap could be realized, and it was possible to change the devices only for any test, instead of the removing entire model, with large set-up time savings. The driving cab was divided into two symmetric shell parts, glued together to maintain a smooth surface and obtain a light model. The tractor and the trailer were screwed together, not allowing any relative motion. The target vehicle scaled model overall dimensions (without the mirrors) are reported in Table 1.

2.2. Front-rear trailer device

The tested devices consisted of aerodynamic appendages to be installed on the front and rear of the trailer, as reported in Fig. 5. The shape optimization of the Front-Rear trailer device, as well as the number of devices and their position along the trailer length, have already been studied in the author's previous works numerical work (Salati et al., 2015).

The semi-elliptic shape of the Front trailer device was optimized using its length as the leading parameter: all the devices had a fixed height $b = 5$ *cm* (full-scale) while the length a changed from *15 cm* to *45 cm* (full-scale) as reported in Fig. 4.

The devices were positioned along the vehicle length (see Fig. 5-a): front device (device "B"), rear device (device "C") and front-rear device (device "BC"). Devices "B" and "C" were split into a side part and a top part to study which part most affected the overall vehicle drag. The rear device was divided into a top rear device (device "G") and side rear devices (device "E"), while the front one was separated into device "F" and device "D" (see Fig. 5-b).

2.3. Experimental apparatus

The experiments were conducted at the Politecnico di Milano wind tunnel. This wind tunnel is a closed-circuit facility in vertical arrangement having two test sections: one of dimensions *14 m* × *4 m* (low speed boundary layer test section) and the other of dimensions *4 m* × *4 m* (high speed and low turbulence test section). Both the test sections are equipped with a turntable to perform crosswind study. For this study, the high-speed test section was used.

In Table 2, Tunnel test section characteristics are reported. To correctly predict the flow field around the vehicle and cut out the wind tunnel boundary layer, a ground board was positioned under the vehicle on the wind tunnel floor. The board dimensions and shape are shown in Fig. 6, where also the relative position of the vehicle is reported. The ground board used, was modelled and designed following previous authors' works on vehicle aerodynamics to ensure the absence of adverse effects from the spill-over of the surrounding flow and to control the thickness of the boundary layer generated by the ground board itself [as an example 23, 24, 25, 26]. From the works of previous authors and tests, this table is suitable for performing crosswind experiments until a yaw angle of 30°–35° appears.

To measure the aerodynamic forces acting on the vehicle, a six-component industrial dynamometric balance was connected to the instrumented vehicle. The balance was located inside the trailer close to the aerodynamic center of the vehicle model (see Fig. 3-b) to minimize the aerodynamic moments on the balance itself. It was connected to the vehicle by an iron plate of thickness *2.0 cm*. The balance and the wind tunnel ground were connected by a circular support (diameter *30 mm*) that was fixed to the balance and which passed through the bottom of the trailer (see Fig. 3-b). The range for each force component and the corresponding maximum error on full scale values are summarized in Table 3.

Several experiments were made to compute the errors associated with the aerodynamic forces at the different tested speeds and yaw angles. The errors associated with the measurements of the aerodynamic forces account for the uncertainties in the flow parameters and in the test procedures. Maximum errors of *2%* for the C_X, *7%* for the C_Y and *5%* for the C_Z were measured. The measurement error was relatively small when the flow speed was increased, suggesting good result reliability and good flow stability.

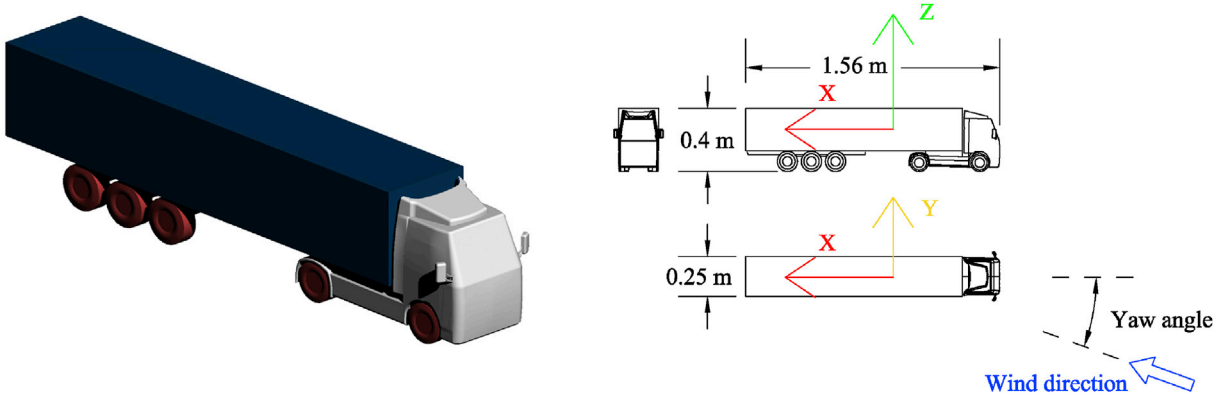

Fig. 2. Heavy truck geometry.

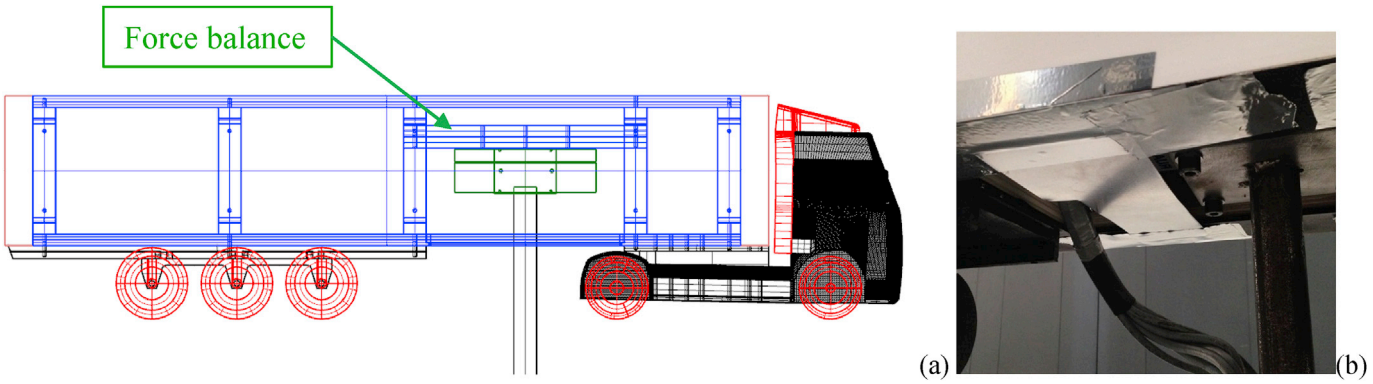

Fig. 3. Force balance inside the trailer (a), detail of the connection between the truck and the trailer (b).

Table 1
Model overall dimension.

length [m]	Width [m]	Height [m]
1.56	0.25	0.40

The set-up, the model, the ground board and the experiment procedure match most indications of SAE standard J1252 (SAE International Surface Vehicle Recommended Practice, 1979).

The model was developed in a way that made it possible to install/remove the device with the vehicle placed in the testing position, without the need to remove the entire vehicle and the balance. In Fig. 3-a, the supports for the aerodynamic devices are shown in pink, the OSB frame in blue and the force balance inside the trailer in green.

The drag (F_X), side (F_Y) and lift (F_Z) forces were computed as the force applied to the vehicle in directions x, y and z, according to the reference system reported in Fig. 6. The HGV aerodynamic force coefficients were calculated as follow:

$$\begin{aligned} C_X &= -\,\text{Blockage} * \frac{F_X}{0,5{*}\rho{*}U_\infty^2{*}A_{res}} \\ C_Y &= \quad\text{Blockage} * \frac{F_Y}{0,5{*}\rho{*}U_\infty^2{*}A_{res}} \\ C_Z &= \quad\text{Blockage} * \frac{F_Z}{0,5{*}\rho{*}U_\infty^2{*}A_{res}} \end{aligned} \tag{1}$$

where ρ is the air density, U_∞ is the speed of the air, A_{res} is the frontal area of the vehicle for both front wind and crosswind. The vehicle and table blockage effects were computed using the Maskell theory (Maskell, 1963), where A is the projecting frontal area of the vehicle and of the ground board, while S is the working section area. The blockage correction it is applied C_X, C_Y snd C_Z. This correction is the one that best fits the experimental results for the wind tunnel used [as an example 23, 24, 25, 26].

$$\text{Blockage} = 1\text{–}2.5\ A/S \tag{2}$$

2.4. Experimental tests program

The first tests were performed on the target truck (see Fig. 5-a) to define the reference data for windward and crosswind conditions at different wind speeds. Tests were performed using wind speeds of *15*, *30*, *50 m/s,* to verify possible Reynolds effects, and at yaw angles (the yaw angle is the angle existing between the vehicle speed and the wind direction see Figs. 2 and 6) between *-30°* and + *30°* with steps of *5°* to check the aerodynamic symmetry of the wind tunnel model. The HGV, equipped with devices "B", "C" and "BC" (devices B and C installed together on the trailer) was tested with yaw angles between *0°* and *15°* in steps of *5°* and a wind speed of *30 m/s* and *50 m/s*.

Devices "D", "E", "F", "G" (see Fig. 5-b) were tested with *0°* and *10°* yaw angles at *30 m/s* and *50 m/s*. Finally, the performance of device "B" having different lengths was examined (see Figs. 4 and 7-e): length "a" from *15 cm* to *45 cm* full-scale (see Fig. 4) with *0°* and *10°* yaw angles at *30 m/s* and *50 m/s*. All the results were then compared with previous CFD results reported in Salati et al. (2015).

To avoid issues with the boundary layer generated by the ground board, and to prevent contact between the model and the ground itself during the tests, the clearance gap was set at 0.5–1 cm and was kept constant during the whole experimental campaign.

Table 4 summarizes the overall program of the experiment.

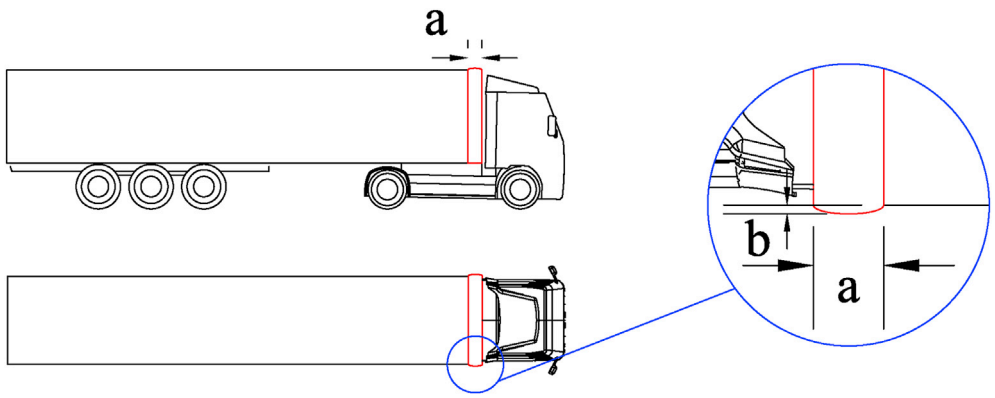

Fig. 4. Front trailer device installed on the trailer.

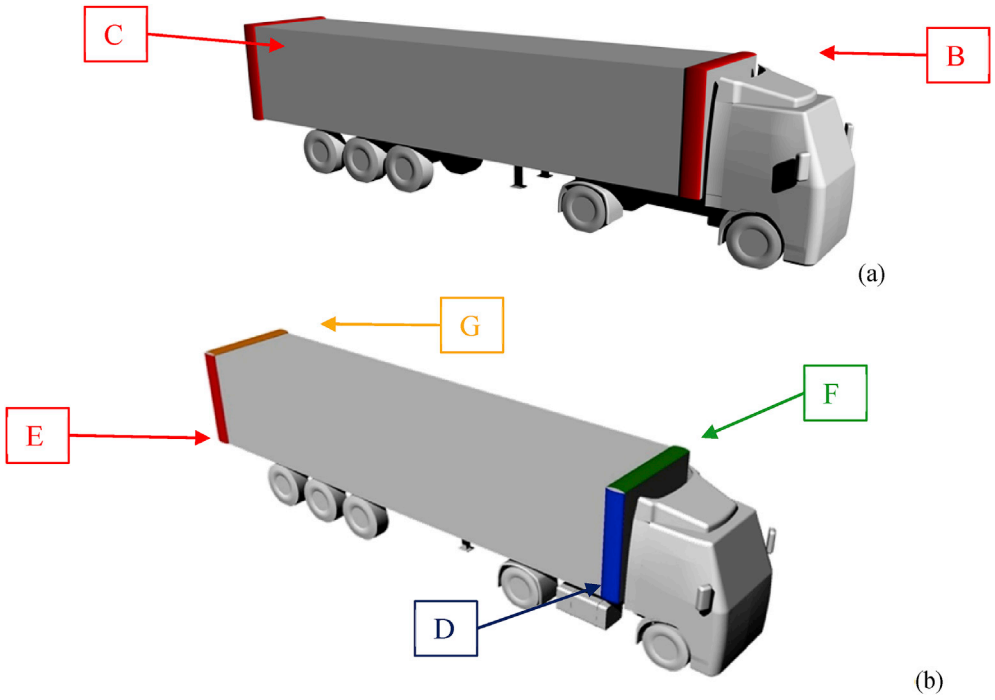

Fig. 5. Device position along the vehicle length: devices B and C (a), devices D, E, F, G (b).

Table 2
Wind Tunnel test section characteristics.

Test Section	Size [m]	Max speed [m/s]	Longitudinal turbulence intensity Iu [%]
Boundary layer	14 × 4	16	<2.0
Low turbulence	4 × 4	55	<0.2

3. Results and discussion

3.1. Target vehicle

As mentioned in the previous section, some preliminary tests were performed on the target vehicle at different yaw angles to obtain the reference data. In general, when the yaw angle is increased, the aerodynamic force raises consequently. In particular, the lateral force coefficient (C_Y - force in the y direction according to the reference system in Fig. 6 and equation (1) raises linearly with respect to the yaw angle, while the drag coefficient (C_x-force in the x direction according to the reference system in Fig. 6) has a minimum yaw angle of *0°* and increases until *25°*. The variation of the aerodynamic forces over the yaw angle agrees with other works in literature, among which Argentini et al. (2011). Looking at Fig. 8, a general agreement between the results obtained at the different tested speeds was found, even if some Reynolds effects could be seen between the wind speeds of *15-30 m/s* and *50 m/s* in the aerodynamic forces, something that will be further discussed. All the presented results were corrected with the experimental blockage correction generated by the truck and the flat ground.

Table 3
Force balance full scale values and error.

± Fx [N]	± Fy [N]	± Fz [N]	± Mx [Nm]	± My [Nm]	± Mz [Nm]	ε_a [%]
1500	1000	5000	500	1000	600	0.05

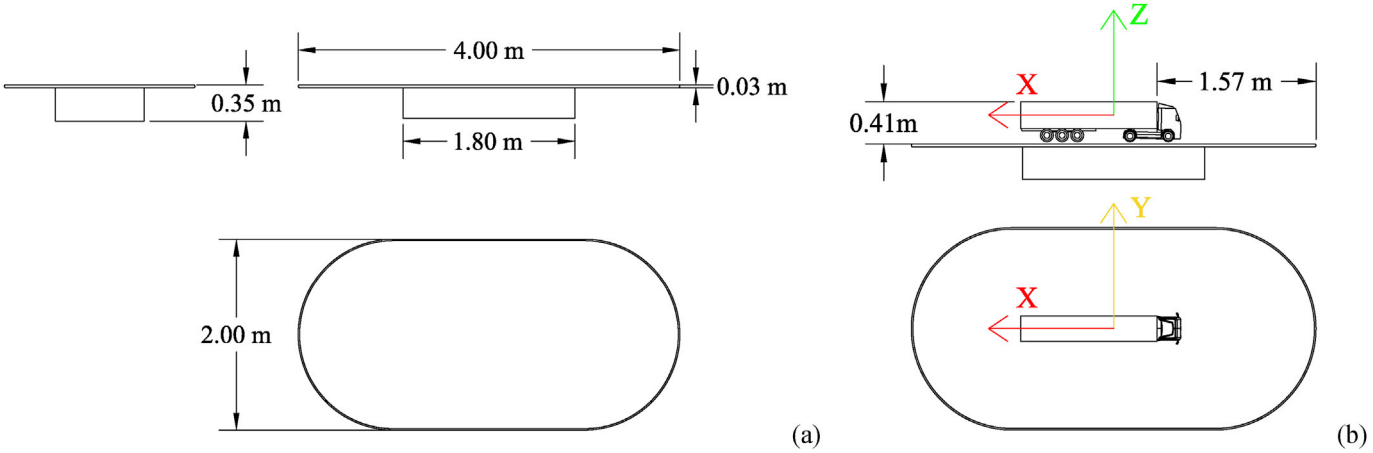

Fig. 6. Ground board: ground board dimensions (a), relative position between the ground board and the vehicle (b).

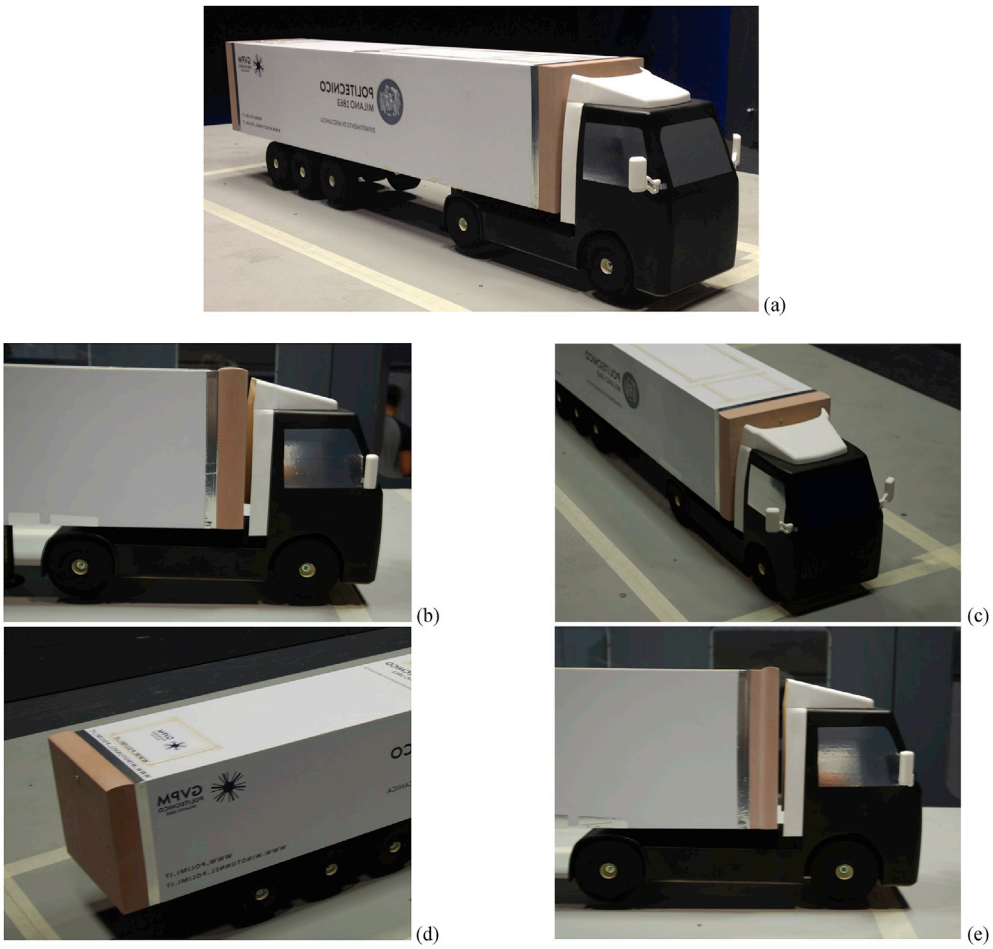

Fig. 7. Target vehicle (a), device "B", $a = 0.45$ m (b), device "D", $a = 0.45$ m (c), device "G", $a = 0.45$ m (d), device "B", $a = 0.25$ m.

Table 4
Design of experiment matrix, with the summary of the main tested parameters.

Velocity [m/s]	Yaw angles [deg]	Device Code	Description
15 30 50	−30 −25 −20 −15 −10 −5 0 5 10 15 20 25 30	A	Target Vehicle
30 50	0 5 10 15	B	Front-device (a = 45 cm)
30 50	0 5 10 15	B + C	Front-Rear trailer device (a = 45 cm)
30 50	0 5 10 15	C	Rear trailer device (a = 45 cm)
30 50	0 10	D	Front trailer device side (a = 45 cm)
30 50	0 10	D + E	Front rear trailer device side
30 50	0 10	E	Rear trailer device side
30 50	0 10	F	Front trailer device top
30 50	0 10	F + G	Front rear trailer device top
30 50	0 10	G	Rear trailer device top
30 50	0 10	B	Front-device (a = 35 cm)
30 50	0 10	B	Front-device (a = 25 cm)
30 50	0 10	B	Front-device (a = 15 cm)
30 50	0 10	B + C	Front-Rear trailer device (a = 35 cm)

The experimental results are compared with a previous numerical study performed by the authors (Salati et al., 2015)on the same vehicle: the numerical analyses were conducted on a 1:1 scale vehicle running at the constant speed of *27 m/s*. Steady state RANS (Reynolds Averaged Navier-Stokes) simulation and transient DES (Detached Eddy Simulation) were performed for several yaw angles (see dashed line in Fig. 8). The numerical simulations were performed with a higher Reynolds number compared to the experiment (a real driving condition was considered (Salati et al., 2015).

The CFD results, especially those of the DES, matched the experimental ones, nevertheless the truck had rotating wheels and moving ground in the CFD while both these conditions were missing in the experiment. These differences can be observed especially at the 0° yaw angle. Following the work of Stapleford and Carr (1969) on a fully exposed wheel, the C_Z and the C_X given by a rotating wheel with zero ground clearance were found to be approximately those of a fixed wheel with small ground clearance, even lower in this case where most of the wheels were shielded from the wheelhouse (in the tractor) and from each other (in the trailer). On the contrary, the absence of moving ground in the experiment influenced the flow field in the underbody of the vehicle. This aspect can be noticed especially at the zero yaw angle, where higher differences were observed between numerical simulations and the wind tunnel test. When the yaw angle rises, the flow field around the vehicle is mostly affected by separation over the leading upper edge of the trailer, not the underbody.

The aerodynamic forces reported in Fig. 8, suggest the presence of some Reynolds effect between the wind speed of *15-30 m/s* and *50 m/s*, especially when the yaw angle rises after *10°-15°*. The authors believe that part of this Reynolds effect can be imputed to the separation of the flow on the windward side of the trailer and part is generated by the flat ground itself: when the yaw angle increases, the effect of the table

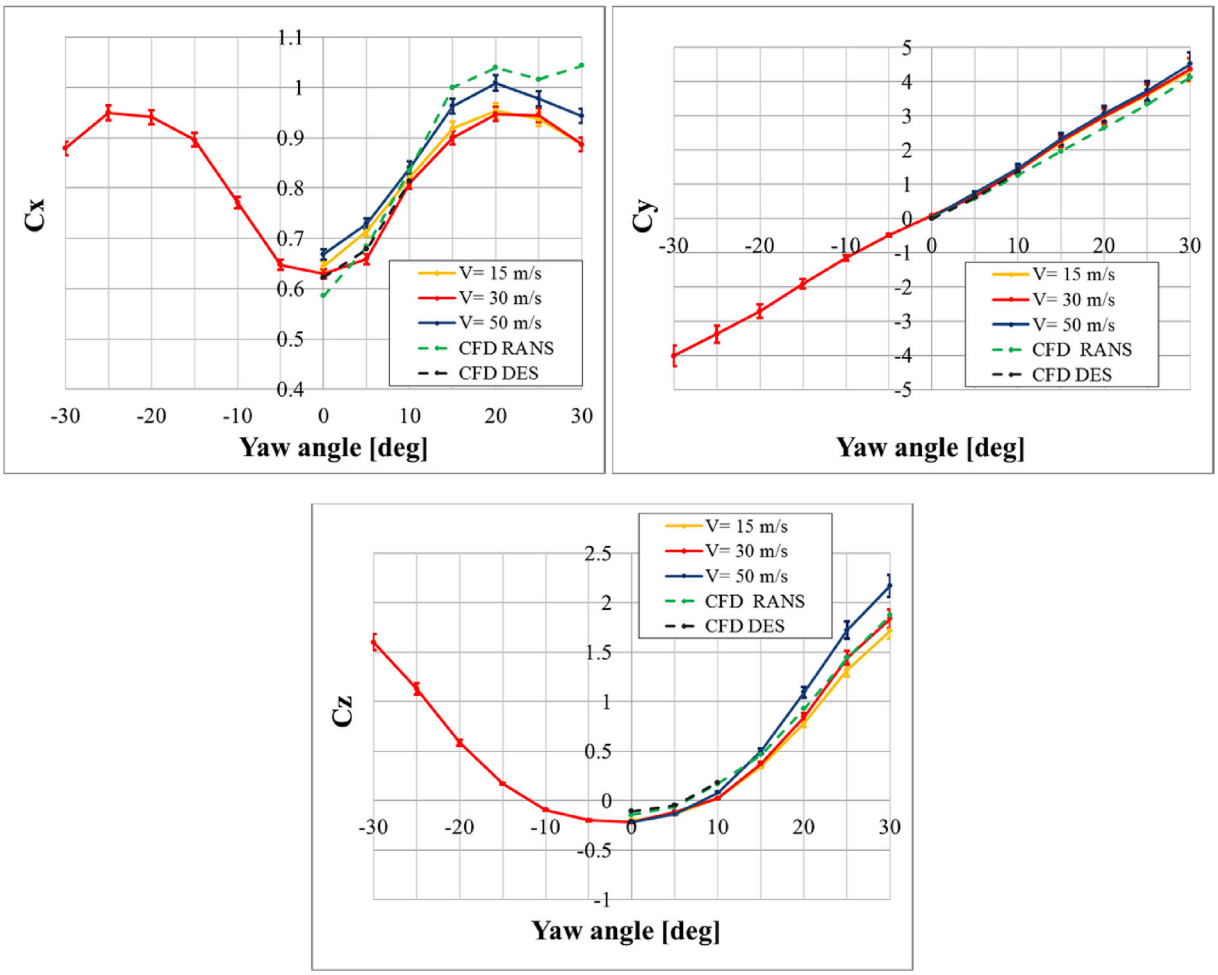

Fig. 8. Comparison between the experimental aerodynamic coefficients and numerical results (CFD RANS and CFD DES from Salati et al (Salati et al., 2015).) on the target vehicle.

aerodynamics on the HGV also increases as a result of the table geometry.

The measured experimental C_X and the calculated numerical one are consistent with each other. Small differences between numerical and experimental results can be seen in the slope of the curve of the side force coefficient C_Y over the yaw angle.

A good correspondence of the results was observed also for the lift force coefficient C_Z; in particular, it is possible to visualize how the lift coefficient changes the sign from negative to positive when the yaw angle increases from *0°* to *10°* in both the wind tunnel tests and the CFD.

3.2. Front-rear trailer device

In this section, the performance of devices "B", "C" and "BC" (see Fig. 9-a) are reported and compared with the numerical results, following the test program reported in Sections 2 and 3. Fig. 9, shows the variation of the C_X with respect to the yaw angle for the two different tested speeds: continuous lines are used for the wind tunnel results while dashed lines report the numerical results of the DES simulations.

The drag force coefficient C_X increases with the yaw angle and a general agreement between the wind tunnel and CFD results can be observed. The CFD simulation generally predicts lower aerodynamic forces and higher device performance than the experiment. Nevertheless, in both numerical simulation and experiments, the device performance decreases when the yaw angle rises. Looking at the aerodynamic efficiency of the devices, a similar drag reduction between the experiments and the numerical results of the device "B" can be seen: the numerical analysis predicted a drag reduction of *6%* in this configuration (Salati et al., 2015).

As described in previous works of the authors (Salati et al., 2015), the device influences the flow in the tractor-trailer gap, allowing a better flow over the two objects and producing less turbulence over the trailer length (top and sides of the trailer). The authors believe that the positive effects of the device will be even greater in a real driving condition, where there is a difference between the oscillation of the tractor and that of the trailer due to vehicle handling.

On the contrary, the measured performance of device "C" disagrees with that of the simulations (in the CFD a drag reduction of around 6% was obtained in this configuration). Even if smaller, these differences are also visible when the device "BC" is mounted on the trailer: the CFD predicted a drag reduction of around *12%* while in the experiments a drag reduction of around *9.5%* was obtained.

As discussed in Section 3.1, both moving ground and rotating wheels that influence the flow in the underbody of the vehicle are not present in the wind tunnel experiment. Device "E" (the side part of device "C") is the one that showed the least performance, suggesting that the fluid leak, from the underbody of the vehicle to its rear-sides, is especially influenced by the different boundary conditions. In fact, when a DES simulation is run in a similar manner to that indicated by Salati et al. (2015). and with the boundary condition used in the experiment, similar behavior for device "C" is observed between the simulations and the experiment.

The results in Fig. 9 and Table 5, suggest the presence of some Reynolds effect when the wind speed raise from *30 m/s* to *50 m/s*. Nevertheless, the drag reduction is constant at both the tested wind speeds and at any yaw angle. At a speed of *30 m/s,* the front device (device "B") decreases the HGV drag by about *8%* while the rear one (device "C")

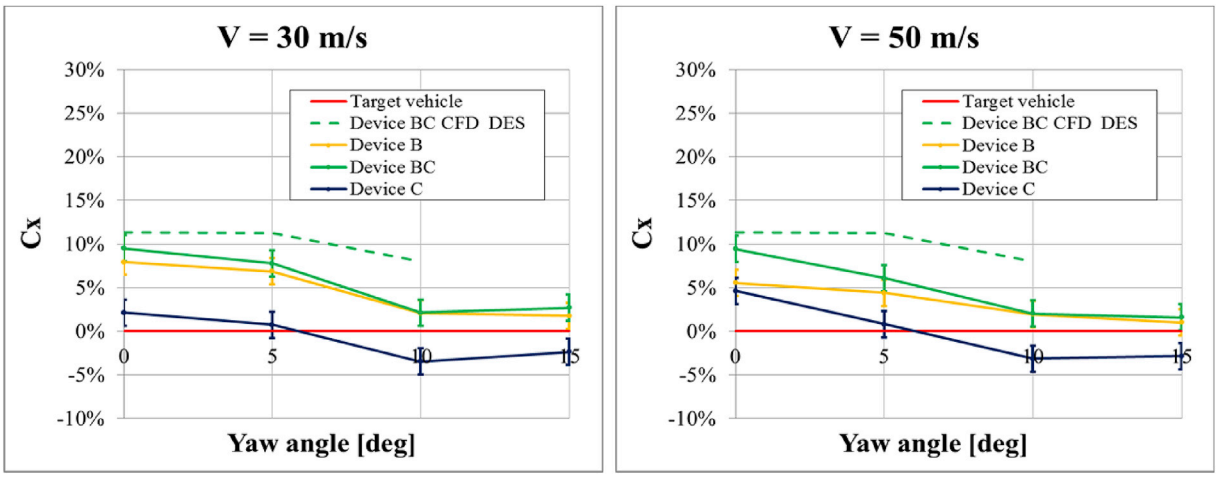

Fig. 9. Comparison between the experimental aerodynamic forces and the numerical ones on the vehicle equipped with devices "B", "C" and "BC" (see Fig. 5-a).

Table 5
Drag reduction for the tested devices.

	V = 30 m/s		V = 50 m/s	
Device	C_X	C_X Reduction	C_X	Cx Reduction
B	0.58	8%	0.63	6%
BC	**0.57**	**10%**	**0.61**	**9%**
C	0.62	2%	0.64	5%
D	0.60	5%	0.64	4%
D + E	0.61	4%	0.64	4%
E	0.62	1%	0.65	2%
F	0.61	3%	0.65	2%
F + G	0.60	4%	0.64	5%
G	0.63	1%	0.63	6%

reduces the drag by about *2%*. On the contrary, when device "B" is installed, the drag reduction at a speed of *50 m/s* is about *5.5%*, while it is about *4.6%* when the vehicle is equipped with device "C". When both devices are mounted on the vehicle, a drag reduction of about *9.5%* is observed. This consideration suggests that the front-trailer device will work and will perform well at different vehicle speeds. Increasing the vehicle speed means that the front device will produce lower drag reductions that are compensated by the higher drag reduction of the rear device. On the other hand, at all tested speeds the rear device always performs less well than the device computed from the numerical studies. The authors believe that it is mainly a problem of different boundary conditions between the numerical simulation and the experiment.

When the front and rear trailer devices are decomposed into devices "D", "E", "F" and "G" (see Fig. 5-b), it is possible to see that the main contributions of drag reduction are given by the front device "D" when installed laterally. The same is true for device "F" when installed on the top at lower Reynolds numbers, and for device "G" with higher speeds. Looking at devices "D" and "F", there is a constant drag reduction at both the tested speeds, while device "G" only works when the vehicle speed increases.

It can also be noticed that the combination of only side devices (front and rear called device "D + E") or the top device (front and rear called device "F + G") can reduce the drag (around *4%*) consistently. This configuration can be suitable for the homologation procedure: in some countries, increasing the maximum vehicle height can be problematic, while in others, the HGV width can be critical.

At both tested speeds, the combination of devices "D + E" and "F + G" gave a constant drag reduction, suggesting that they might work correctly at different vehicle speeds. As previously shown with devices "C" and "B", when the vehicle speed increases, the front devices have a lower performance that is compensated by the increase in performance of the rear one. This, of course, should be confirmed with some road test.

3.3. *Device shape optimization*

In this section, the shape of the front trailer device (device "B") was optimized using the length of the device itself as a leading parameter (see Fig. 4), following the test program reported in Section 2.4.

The results for the target vehicle are reported using a dashed line:

- blue dashed line – C_x of the target vehicle at *50 m/s*;
- red dashed line – C_x of the target vehicle at *30 m/s*;
- green dashed line – C_x of the target vehicle computed in previous authors' works (Salati et al., 2015).

In general, when the device is installed, a reduction of the C_x is observed with any of the tested devices (see Fig. 10) and a similar monotonic behavior is found, suggesting that the device which provides the higher performance is the longer one. Bigger devices are not taken into consideration due to the higher production and installation costs resulting from the increases in volume and weight.

Once again, the results suggest the presence of some Reynolds effect when the wind speed is increased from *30 m/s* to *50 m/s* (see Fig. 10). CFD analysis predicts the optimal device length as being *0.45 m*, with a similar result obtained in wind tunnel tests at a wind speed of *30 m/s*. At

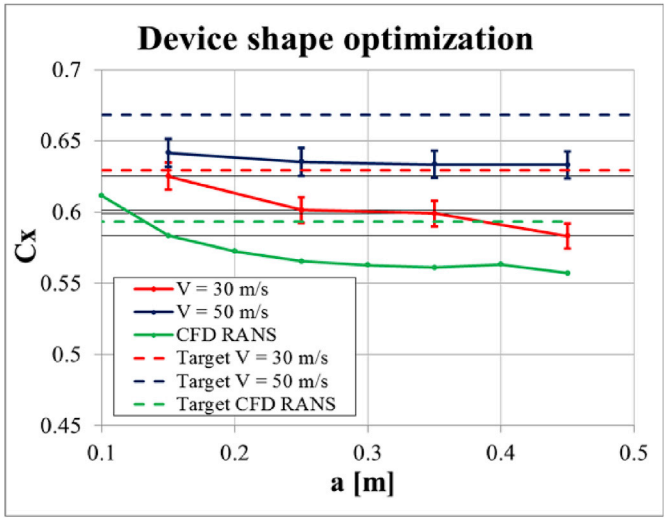

Fig. 10. Front trailer device sensitivity to the length *a* (see Fig. 4).

the highest wind velocity, the performances of the device are almost constant at all lengths. This test suggests that even if the device length has a limited influence at higher Reynolds numbers, the optimum length of *0.45 m* is the most suitable one for several different vehicle speeds.

4. Conclusion

In this paper, wind tunnel tests were performed on a heavy goods truck equipped with a Front-Rear trailer device previously developed using a CFD approach by the authors (Salati et al., 2015). The results show good agreement between the numerical calculations and the experimental measured data. The obtained maximum drag reduction is about 9.5% when both the front device and the rear one are installed on the truck. The optimum length of the device is about 45 cm. The device gives a drag reduction both in front and crosswind conditions. The lateral and vertical forces acting on the vehicle do not change significantly, indicating that there are no critical issues for vehicle handling and stability in crosswind.

It can also be noticed that the combination of only side devices (front and rear called device "D + E") or the top device (front and rear called device "F + G") can reduce the drag (around *4%*) consistently. This configuration can be suitable for the homologation procedure: in some countries, increasing the maximum vehicle height can be problematic, while in others, the HGV width can be critical.

The authors believe that the impact of the developed device will be higher in cases in which the trailer and the tractor are made by different producers and are not integrated with each other as normally occurs with most heavy trucks. They help the flow-fields in one of the most critical areas of drag reduction: the gap between the driving cab and the trailer. Nevertheless, this device can also be a good strategy for reducing the aerodynamic forces acting on a container, where the shear stress and the drag sources are much higher than on a standard trailer.

References

Argentini, T., Ozkan, E., Rocchi, D., Rosa, L., Zasso, A., 2011. Cross-wind effects on a vehicle crossing the wake of a bridge pylon. J. Wind Eng. Ind. Aerodyn. 99 (6–7), 734–740. https://doi.org/10.1016/j.jweia.2011.01.021. ISSN 0167-6105.

Buchheim, R., Deutenbach, K., Lückoff, H., 1981. Necessity and Premises for Reducing the Aerodynamics Drag of Future Passenger Cars. SAE Technical Paper 810185. https://doi.org/10.4271/810185.

Cooper, K., 2003. Truck Aerodynamics Reborn - Lessons from the Past. SAE Technical Paper 2003-01-3376. https://doi.org/10.4271/2003-01-3376.

Dávila, A., Nombela, M., 2011. Sartre - Safe Road Trains for the Environment Reducing Fuel Consumption through Lower Aerodynamic Drag Coefficient. SAE Technical Paper 2011-36-0060. https://doi.org/10.4271/2011-36-0060.

Drollinger, R., 1987. Heavy Duty Truck Aerodynamics. SAE Technical Paper 870001. https://doi.org/10.4271/870001.

Garry, K.P., 1981. Development of container-mounted devices for reducing the aerodynamics drag of commercial vehicles. J. Wind Eng. Ind. Aerodyn. 9, 113–124. https://doi.org/10.1016/0167-6105(81)90082-9.

Garry, K.P., 1985. A review of commercial vehicle aerodynamics drag reduction techniques. Proc. Inst. Mech. Eng. D Transp. Eng. 199, 215–220. https://doi.org/10.1243/PIME_PROC_1985_199_159_01.

Gilhaus, A., June 1980. "The influence of cab shape on air drag of trucks. In: Presented at the 4th Colloquium on Industrial Aerodynamics, vols. 1–20, pp. 133–156. Aachen.

Howell J., "The influence of ground simulation on the aerodynamics of simple car shapes with an underfloor diffuser," Presented at the RaeS Conference on Vehicle Aerodynamics, Loughborough, July 1994, pp. 36.1-11.

Hucho, W.H., 1987. Aerodynamics of Road Vehicles. Butterworth, ISBN 0408014229. London.

Ingram, K., 1978. The wind-averaged drag coefficient applied to heavy goods vehicles," Transport and Road Research Laboratory. TRRL Suppl. Rep. 392.

Landman, D., Wood, R., Seay, W., Bledsoe, J., 2010. Understanding practical limits to heavy truck drag reduction. SAE Int. J. Commer. Veh. 2 (2), 183–190. https://doi.org/10.4271/2009-01-2890.

Leuschen, J., Cooper, K., 2006. Full-scale Wind Tunnel Tests of Production and Prototype, Second-generation Aerodynamic Drag-reducing Devices for Tractor-trailers. SAE Technical Paper 2006-01-3456. https://doi.org/10.4271/2006-01-3456.

Leuschen, J., Cooper, K.R., 2009. Summary of Full-scale Wind Tunnel Tests of Aerodynamics Drag-reducing Devices for Tractor–trailers. The Aerodynamics of Heavy Vehicles II: Trucks, Buses, and Trains. Springer, New York, pp. 451–462. https://doi.org/10.1007/978-3-540-85070-0_41.

Maskell, E.C., November 1963. A Theory of the Blockage Effects on Bluff Bodies and Stalled Wings in a Closed Wind Tunnel, vol. 340. Ministry of Aviation (UK). Reports and Memoranda R & M.

McCallen, R., Salari Ortega, J., Castellucci, P., Browand, F., Hammache, M. et al., "DOE's effort to reduce truck aerodynamics drag – joint experiments and computations lead to smart design," Presented at the 34th AIAA Fluid Dynamics Conference and Exhibit, AIAA 2004-2249, Portland, June 22, 2004, UCRL-CONF-204819.

Minelli Krajnović, S., Basara, B., Noack, B.R., 2016. Numerical investigation of active flow control around a generic truck a-pillar. Flow, Turbul. Combust. 1573–1987. https://doi.org/10.1007/s10494-016-9760-3.

SAE International Surface Vehicle Recommended Practice, "Wind Tunnel Test Procedure for Trucks and Buses" SAE Standard J1252, Rev. Aug. 1979.

Palowski, F.W., 1930. Wind resistance of automobiles. SAE J. 27, 5–14.

Salati, L., Cheli, F., Schito, P., 2015. Heavy truck drag reduction obtained from devices installed on the trailer. SAE Int. J. Commer. Veh. 8 (2), 747–760. https://doi.org/10.4271/2015-01-2898.

Schito, P., Braghin, F., 2012. Numerical and experimental investigation on vehicles in platoon. SAE Int. J. Commer. Veh. 5 (1), 63–71. https://doi.org/10.4271/2012-01-0175.

Schoon, R., 2007. On-road Evaluation of Devices to Reduce Heavy Truck Aerodynamics Drag. SAE Technical Paper 2007-01-4294. https://doi.org/10.4271/2007-01-4294.

Stapleford, W.R., Carr, G.W., 1969. Aerodynamic Characteristics of Exposed Rotating Wheels. MIRA. MIRA Rep. No. 1970/2.

The Council of The European Union, July 1996. Council Directive 96/53/EC.

Watkins, S., Saunders, J.W., Hoffman, P.H., 1993. Comparison of road and wind-tunnel drag reductions for commercial vehicles. J. Wind Eng. Ind. Aerodyn. 49, 411–420.